$^{240}Pu/^{239}Pu$ isotopic ratio measurements in micrometric Pu and MOX particles using Secondary Ion Mass Spectrometry

Aurélie Diacre, Anne-Laure Fauré, Manon Cornaton, Fabien Pointurier, Olivier Evrard

$^{240}Pu/^{239}Pu$ isotopic ratio measurements in micrometric Pu and MOX particles using Secondary Ion Mass Spectrometry

Aurélie DIACRE[a,b], Anne-Laure FAURE[a], Manon CORNATON[a], Fabien POINTURIER[a], Olivier EVRARD[b]

[a]*Commissariat à l'Energie Atomique et aux énergies alternatives (CEA, DAM, DIF), F-91297 Arpajon, France*

[b]*Laboratoire des Sciences du Climat et de l'Environnement (LSCE/IPSL), Unité Mixte de Recherche 8212 (CEA/ CNRS/UVSQ), Université Paris-Saclay, Gif-sur-Yvette, France*

E-mail: aurelie.diacre@lsce.ipsl.fr

Key words: Hydride formation rate, Hydride correction, RSF determination, Pu quantification.

Abstract

Every accident affecting industrial or nuclear facilities emits micrometric fragments of material into the environment whose elemental and isotopic compositions are characteristic of the process or event. Particle analysis, mainly implemented in the framework of the Non Proliferation Treaty to detect clandestine nuclear activities, provides a powerful tool to identify the origin of the nuclear particulate matter and to assess the environmental impact of nuclear accidents. Initially, particle-scale isotopic analyses aimed at the determination of the U isotopic composition. Now, focus is increasingly given on Pu isotopic measurements to address its origin and potential use. Such measurements are more challenging because of isobaric interferences, including those induced by hydride ions, like $^{239}PuH^+$ on $^{240}Pu^+$ and $^{238}UH^+$ on $^{239}Pu^+$ in Mixed Oxide (MOX). Such ions are generated during ionization processes by Secondary Ion Mass Spectrometry. Based on a parametric study aiming at the measurement of uranium oxide, uranium carbide and uranium single and double hydride rates, we determined that Pu and U should be detected as elementary ions to limit the impact of such

interferences, although mono-oxide ions are more abundant. Thus, we developed an analytical methodology to obtain accurate $^{240}Pu/^{239}Pu$ atomic ratios both for weapon grade Pu and MOX materials. Hydride rate is first measured in U oxide particles and then applied to correct $^{240}Pu^{+}$ and $^{239}Pu^{+}$ signals. The relative difference of corrected $^{240}Pu/^{239}Pu$ isotopic ratios with expected values is reduced by a factor of 4 when measuring weapon grade Pu particles and by a factor of 10–100 when measuring MOX particles containing 1 to 10 wt% of Pu. We also proposed a method to determine the Relative Sensitivity Factor (RSF) based on the decay of Pu in order to quantify the Pu content in MOX samples. The estimated lowest measurable 239Pu/238U atomic ratio in MOX particles is ~1.6×10^{-3}.

1. Introduction

Many industrial activities produce large amounts of particles[1,2], with sizes ranging from a few nm to hundreds of µm. A fraction of these particles may be released into the environment. In the case of nuclear facilities, despite the strict precautions to confine nuclear materials, very small fractions of the particles may be released and they may ultimately settle onto surfaces within the facilities. The molecular, elemental and isotopic compositions of these particles are representative of the processed nuclear materials [3,4], i.e. made of uranium (U) and/or plutonium (Pu), the main chemical elements used in the nuclear industry, both for civilian and military applications. They provide fingerprints of current and past activities in nuclear facilities. Therefore, the analysis of these particles is of major interest for nuclear safeguards. Inspectors of IAEA (International Atomic Energy Agency) regularly collect particulate materials in nuclear facilities by wiping surfaces by means of square pieces of cotton tissues referred to as “swipe samples” [5]. These samples mainly contain environmental and industrial dust and in many cases, a very small amount of particles made of nuclear material. The swipe samples are analysed by a handful of specialized laboratories, members of the IAEA Network of Analytical Laboratories (NWAL), which are able to carry out “particle analysis”, i.e. measurement of the isotopic composition of actinides (mainly U) in individual micro-particles [3,5].

Consequently, precise and accurate methods for particle isotopic measurements were developed in the 1990s in the field of nuclear safeguards. Currently, two methods are implemented within the NWAL. The first method is the combination of the Fission Track (FT) technique and of Thermal Ionization Mass Spectrometry (TIMS) [6–8]. The FT technique allows locating particles containing fissile nuclei under a flux of thermal neutrons (e.g. ^{235}U, ^{239}Pu). Then, the isotopic composition of some of the localized particles are measured by TIMS. The second method is based on the use of the Secondary Ion Mass Spectrometry (SIMS) method, which has been used since the 2000's[9]. SIMS is the only technique that can provide both particle location and isotopic measurements using a single instrument, with a high sensitivity and a high lateral resolution [10]. The development of the Automated Particle Measurement software by Cameca [11,12] allowed the SIMS method to detect and locate U bearing-particles in the whole sample, like the FT-TIMS method. The implementation of the large geometry – SIMS (LG-SIMS) has further improved the performance of isotopic measurements thanks to the increase of the mass resolution (to separate ions of interest from interfering species) and to the use of several detectors for the simultaneous collection of ion beams (multi-collection) [13–15]. Initially, particle analyses only aimed at the determination of the isotopic composition of U. During the past 20 years, other methodologies were developed to measure other characteristics of the U particles than their isotopic composition, for instance fluorine content [10], abundance of the ^{230}Th progeny of ^{234}U to "date" U (i.e. determine the date of the last chemical purification of the U material) [16], minor and major elemental constituent of the particles by SEM-EDS (Scanning Electron Microscope- Energy Dispersive Spectroscopy)[17], chemical phases of the U compounds by micro-Raman spectrometry[17], etc.

Beyond U particle measurements, detection and characterization of Pu in particles is also of uttermost importance for nuclear safeguards, as Pu is also widely used in the nuclear industry. In addition to pure Pu compounds (PuO_2 for instance), Pu is present in irradiated U, and in mixed U–Pu oxide fuel (i.e. MOX). Futhermore, this element can be found in the environment as a consequence of (1) weapon accidents such as Thule and Palomares [[18,19], (2) chronic discharges from nuclear

78 facilities like Sellafield [20], (3) atmospheric nuclear weapon tests[21] or (4) the Chernobyl (CNPP) [22]
79 and Fukushima Dai-Ichi (FDNPP) [23] accidents. During some of these events Pu was emitted in the
80 form of "Hot Particles" [19,22,24–26], they are defined in 1994 as radioactive particles with a size
81 smaller than 100 µm and an activity higher than 4 Bq [27,28].
82 The measurement of the isotopic composition of Pu in Pu-bearing particles is essential as it enables
83 to identify the source of Pu as well as its origin and potential use (irradiated fuel, MOX fuel for civilian
84 reactors, nuclear weapons, etc.) [29]. Isotopes of potential interest are ^{238}Pu, ^{239}Pu, ^{240}Pu, ^{241}Pu and
85 ^{242}Pu. The most abundant isotopes are generally ^{239}Pu and ^{240}Pu. However, the Pu isotope analysis by
86 SIMS is difficult because of isobaric interferences[29], especially (1) when Pu is present as trace or
87 minor element in an U matrix like in MOX fuel or irradiated fuel, or (2) in the case of weapon grade Pu
88 where the ^{240}Pu concentration is low. In the first case, there is a strong interference of ^{238}UH on ^{239}Pu
89 and in the second case the main interference comes from ^{239}PuH on ^{240}Pu. It is necessary to correct for
90 this hydride contributions to calculate accurate isotopic ratios and this will be investigated in the
91 current research. The first analyses of Pu particle by SIMS were carried out by Betti and al [30] without
92 hydride formation rate correction. More recently, attempts to produce and characterize reference
93 PuO_2 and MOX particles have been performed by Ranebo et al [31]. Other weapon grade Pu particles
94 or MOX particles were also measured by SG-SIMS [31] and LG-SIMS [32]. No hydride correction was
95 performed in these studies to the best of our knowledge. Ranebo et al [31] estimated the Pu hydride
96 formation rate from synthetic Pu particles doped with ^{242}Pu and estimated the U hydride rate from the
97 ^{242}Pu/^{238}U isotopic ratio measured by Isotopic Dilution-TIMS. Nevertheless, these hydride formation
98 rates were not used to correct measured isotopic ratios, which results in some deviations in the
99 isotopic composition of the starting material. Aleshin et al [32,33] also observed a significant negative
100 bias on the ^{240}Pu/^{239}Pu isotopic ratio measured on MOX particles, due to the ^{238}UH interference.
101 Ranebo et al [34] estimated the U hydride rate measured in particles coming from nuclear weapon
102 material remaining from the Thule accident and assumed that this U hydride ratio is valid for Pu
103 hydride formation. Nevertheless, they did not apply any correction on their results and only gave an

interval of $^{240}Pu/^{239}Pu$ atomic ratios based on the estimation of the U hydride formation rates. In the current research, we proposed a methodology to correct for the both U and Pu hydride formation rates in order to improve the accuracy on $^{240}Pu/^{239}Pu$ isotopic measurements conducted on both pure Pu and MOX particles. We also developed a methodology to quantify Pu in MOX particles based on the measurement of the Relative Sensitivity Factor (RSF). Previous studies described attempts to determine such factor from MOX particles but results showed that this factor exhibited large fluctuations during analysis or that they were not reproducible from one particle to the other [22,35]. Here we determined this factor on pure Pu particles based on the measurement of $^{235}U/^{239}Pu$ analysed in "old" Pu particles (i.e. made with Pu purified in 1963), ^{235}U being the progeny of ^{239}Pu. Such determination of the RSF was also used by Wallenius et al [35] to determine the age of Pu particles. The originality of our methodology is to apply this RSF to the quantification of Pu.

The analysis described in this article were carried out on pure Pu or MOX particles in order to demonstrate the feasibility of our methodology and to avoid other isobaric interferences that can be caused by neighboring mineral or metallic particles usually found in real-life sample[14].

Overall, the objectives of the current research are the following:

(1) To determine the optimal U and Pu ionic species to perform U and Pu isotopic measurement in mixed U-Pu bearing particles. UO^+ ions being more abundant than U^+ ions[23,36], it may be better to perform isotopic measurement using mono oxide ions for both U and Pu. However, such ions may also be more subject to isobaric interferences such as $^{239}PuC^+$ on $^{235}UO^+$, $^{238}UOH^+$ on $^{239}PuO^+$. We proposed here a comprehensive parametric study on U particles in order to determine the formation rate of molecular U ions such as oxide, carbide, hydride, etc., to identify the most appropriate ones to characterize MOX particles. In this case, analyses were performed on U particles with different chemical forms (U_3O_8 and UF_4) to study the impact of this parameter on the ion formation rates.

(2) To develop a method to correct the hydride effect on the $^{240}Pu/^{239}Pu$ isotopic ratio in pure Pu particles. The hydride correction factor can be easily measured in pure U particles by calculating the

isotopic ratio $^{238}UH^+/^{238}U^+$. In pure Pu particles, it is not possible to determine the Pu hydride formation rate because of the isotopic composition of this element[34], i.e. presence of ^{240}Pu that interferes with ^{239}PuH. We proposed here to extrapolate the U hydride correction factor to Pu for correcting $^{240}Pu/^{239}Pu$ isotopic ratios.

(3) To apply the hydride correction method to the simultaneous determination of the isotopic composition of U and Pu in MOX samples. For that purpose, the influence of the Pu content on the Pu isotopic measurements was also studied.

(4) To provide a methodology to quantify the Pu content in MOX particles by the determination of the Relative Sensitivity Factor (RSF)

2. Materials, sample preparation and instrumental settings

2.1. Reference materials

Three types of samples were analysed: pure U particles, pure Pu particles and mixed U-Pu particles. Pure U particles from Certified Reference Materials (CRM), NBS U-100 and U-17B (New Brunswick Laboratory, Illinois, USA) were analysed for the parametric study aiming at the determination of the hydride, oxide, carbide, and hydroxide formation ratios on different chemical forms of U. CRM NBS U-100 and CRM U-17B are powdered materials made of tri-uranium octoxide, U_3O_8, and uranium tetrafluoride, UF_4, respectively.

Pure Pu particles from one of the samples of a nuclear forensic exercise (CMX-6 exercise or 6th Collaborative Material Exercise, organized by the International Technical Working Group on Nuclear Forensics) were analysed for the determination of their Pu isotopic composition. This sample consisted of a metal ingot whose surface was contaminated with weapon grade Pu particles. The measurement of the $^{240}Pu/^{239}Pu$ in such Pu compounds is difficult due to their low ^{240}Pu concentration. This sample was also used to determine the Pu/U relative sensitivity factors (RSF) according to previously described methods[29].

155 The simultaneous determination of U and Pu isotopic compositions and the Pu content in U were
156 carried out with particles from two MOX samples referred to as UKMOX-010 and UKMOX-100. These
157 samples are composed of low enriched U oxide and reactor grade Pu oxide powders. The U and Pu
158 isotopic compositions of the two samples were identical, only the bulk atomic Pu/U ratio differed
159 (Table 1).

160

161 **Table 1** Reference isotopic atomic ratio of samples with 2-sigma expanded uncertainties. $^{240}Pu/^{239}Pu$
162 atomic ratios are decay-corrected to the date of the analytical sessions.

Isotopic ratio	CMX-6	UKMOX-100	UKMOX-010
$^{235}U/^{238}U$		$(1.5896 \pm 0.0038) \times 10^{-2}$	
$^{240}Pu/^{239}Pu$	$(6.17 \pm 0.18) \times 10^{-2}$	$(2.8666 \pm 0.0002) \times 10^{-1}$	
U/Pu (mass)		119.79 ± 0.15	12.484 ± 0.017

163

164 *2.2. Sample preparation*

165 Micrometric particles from the CRMs NBS U-100 and U–17 B were collected with plastic tips and
166 transferred to cotton cloth (TX 303, Texwipe, NC, USA). Particles from the CMX-6 sample were
167 collected by wiping the surface of the sample with a cotton cloth. Particles were then transferred from
168 the cotton cloth onto a carbon planchet (grade FP2584 Schunk Electrographite SAS, Germany) under
169 a glove bag filled with nitrogen using the Vacuum Impactor technique [10,37]. This method consists in
170 sucking up particles from the cotton cloth and depositing them by impaction onto a carbon planchet
171 beforehand covered with an organic compound, polyisobutylene in nonane, acting as a sticky agent.
172 Micrometric UKMOX-100 particles were received in an ethanol suspension. The ethanol
173 suspension was mixed with collodion (Merck) and deposited onto Lexan® polycarbonate disks
174 (referred to as “deposition disk”). This process was carried out in an ISO 4 clean room facility. Then, an
175 additional Lexan® disk, acting as a solid-state nuclear track detector (SSNTD) and referred to as “FT
176 disk”, was welded onto the “deposition disk”. The disks were then irradiated in the Triga nuclear
177 reactor (Jozef Stefan Institute, Ljubljana, Slovenia) by means of a specific irradiation device made of
178 aluminium vessels filled with heavy water in order to get a well-thermalized neutron flux with a high

fluence, in the 1015 neutron. cm-2 range [38]. Fission fragments are emitted by ^{235}U and ^{239}Pu during fission reaction, they impacted into the Lexan® disks and created surface damages [39]. Chemical etching of the "FT disk" using KOH solution at 80°C during 15 min enabled to make visible the sea urchin-shaped fission track clusters characteristic of the presence of a fissile nuclide-bearing particle (as described by Diacre et a l. [40]). Thanks to appropriate landmarks on both deposition and FT disks, the particles that produced fission track clusters were localized. These particles were then micro sampled with a tungsten carbide needle under an optical microscope and deposited onto a carbon planchet in an ethanol-ether droplet previously deposited on it (Supplementary information A). This droplet also dissolved the collodion that could induce charging effect during SIMS measurements. At the end of the micro-sampling step, the carbon planchet was heated in an oven at 400°C during 30 min to remove all organic compounds that may generate isobaric interferences [41].

UKMOX-010 micrometric particles were already loaded onto a carbon planchet by direct smearing according to Aleshin et al. [32].

2.3. Instrumental settings

A Secondary Ion Mass Spectrometer (IMS-7f, Cameca Ametek, France) was used for isotope ratio measurements. This instrument was equipped with an oxygen ion source called duoplasmatron. A primary ion beam of oxygen ions was typically used to enhance the production of electropositive ions such as U^+ or Pu^+. All measurements described in this article were carried out with the O_2^+ primary beam accelerated to 15 keV. The positive secondary ions were accelerated to 5 keV. The energy band-pass was set at 75 eV. The contrast and field apertures were respectively 400 µm and 1800 µm and the field of view was 75 µm to enhance the transmission. The mass resolution was set to 400 to obtain flat top peaks and a good sensitivity, which improved the accuracy and the reproducibility of the measurements. Ion species were recorded in a magnet peak jump (PJ) sequence using a single electron multiplier detector (AF150H EM by ETP Electron Multipliers Pty Ltd.). Dead time was experimentally determined to be 32 ns. Raw count rates were corrected for dead time and for time linear drift. Both

U and Pu isotopic ratios were corrected for the same instrumental mass fractionation factor per mass unit, IMF_{amu}, measured on NBS U-100 particles. This factor was calculated according to Eq 1.

$$IMF_{amu} = \left(1 - \frac{\left({}^{U235}/_{U238}\right)_{measured}}{\left({}^{U235}/_{U238}\right)_{certified}}\right) \times \frac{1}{M_{U238} - M_{U235}} \quad (1)$$

with M_{U238} and M_{U235} are the molar masses of ^{238}U and ^{235}U, respectively.

In the literature, a similar approach was used to correct Pu isotopic ratios for mass fractionation effect [42,43]. The accuracy of these corrections on Pu measurements are discussed in the Results and Discussion section. The microbeam settings and the measured ion species used for the different studies described in this article are summarised in Table 2.

Table 2 IMS-7f micro beam settings used for the studies described in this article.

Type of measurement	**Detector used**	**Primary beam**	**Primary beam intensity**	**Raster area**	**Mass resolution (10% level)**	**Impact energy**	**Secondary extraction voltage**
PJ	EM (ETP)	O_2^+	250 pA	No	400	10 kV	5 kV
Objective of the measurement	**Parametric study for identification of the most appropriate ion species**		**Pu isotopic measurement and RSF determination**			**Measurement of U and Pu isotopic compositions in MOX samples**	
Isotopes (integration time in seconds)	^{238}U (1.04), $^{238}U^{1}H$ (2), $^{238}U^{2}H$ (3.04), $^{238}U^{12}C$ (2), $^{238}U^{16}O$ (1.04), $^{238}U^{16}O^{1}H$ (2)		^{235}U (3), ^{236}U (3), ^{239}Pu (1.04) , ^{240}Pu (1.04)			^{235}U (2), ^{238}U (1), ^{239}Pu (3) , ^{240}Pu (4)	
Number of cycles	30		30			30	

3. Results and discussion

3.1. Parametric study for determination of the most appropriate ionic species to perform U and Pu isotopic analyses

The main difficulty when measuring the isotopic compositions of U and Pu in MOX samples came from the isobaric interferences generated by molecular ions made of U or Pu and light elements (H, O, C). The parametric study aiming at determining (1) the U hydride, carbide, oxide and hydroxide

formation rate and (2) the most appropriate U and Pu ionic species to measure isotopic ratios while minimizing isobaric interferences.

The carbide, oxide, hydride and hydroxide formation rates for particles from two U compounds were plotted in Fig. 1. The $^{238}U^{16}O/^{238}U$ ratios presented in Fig. 1A. were above 1 whatever the U chemical form. Even if the oxide formation rate were slightly higher for U_3O_8 particles, these results suggest that the oxygen ions came mainly from the O_2^+ ions of the primary ion beam. The fact that the signal from UO^+ was higher than that from U^+ confirms results previously described in the literature[36,43]. The UC/U^+ ratios presented in Fig. 1B. were below 10^{-3} whatever the U chemical form. UC ions might be generated by the recombination of U ions with carbon coming from the carbon planchet. The UH^+, UH_2^+ and UOH^+ formation ratios were plotted in Fig. 1C. The UH^+ formation ratios were below 10^{-3}, and UOH^+ formation ratios were $\sim 1.5\times10^{-3}$. The UH_2^+ ratios were negligible. The UH^+ formation ratio depends on several factors such as the sample chamber vacuum conditions and the intrinsic hydrogen content of the sample and of the carbon planchet[44]. Experimentally observed UH^+/U^+ ratios range from 10^{-5} to 10^{-3}.

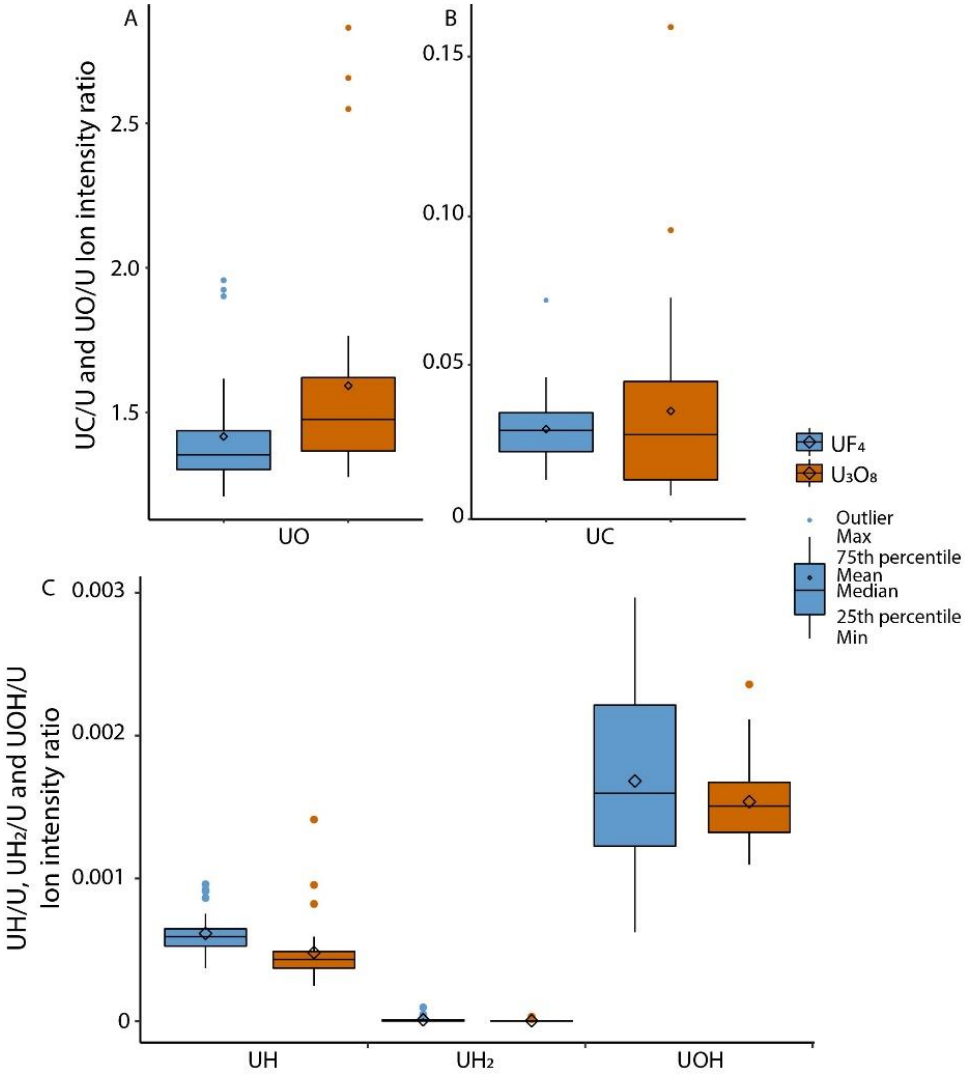

Fig. 1 (A) UC/U; (B) UO/U; (C) UH/U, UH_2/U and UOH/U ion intensity ratios for UF_4 and U_3O_8 particles. Measurements were carried out with a chamber pressure between 1.2 x 10^{-9} and 6.7 x 10^{-9} mbar.

Based on these results, it is apparently better to analyse U in its UO form to increase the sensitivity. However, interference of UO^+ ions with polyatomic ions should also be considered and UO^+ ions may be eventually more interfered than U ions; for instance, $^{235}U^{16}O$ should be interfered by $^{239}Pu^{12}C$. Based on the formation rate measured on pure U particles, we estimate the contribution of the interfering species on the signal of U and Pu for MOX particles. Moreover, we assume that the formation rates of hydride, oxide and carbide ions are equivalent for U and Pu. Regarding the interference of $^{239}Pu^{12}C$ with $^{235}U^{16}O$, the influence of the interference obviously increases with the Pu content in the particle. We calculate the contribution of $^{239}Pu^{12}C$ on $^{235}U^{16}O$ in UKMOX-010 particles

248 containing ~10 wt% of Pu. The $^{239}Pu^{12}C$ signal is ~ 3 % of the total measured signal at 251 m/z, which
249 causes a significant bias in U isotopic ratio if the $^{235}U/^{238}U$ ratio is measured through the $^{235}U^{16}O/^{238}U^{16}O$
250 ratio. Thus, it is preferable to measure U in its elemental form although sensitivity for U^+ is lower than
251 for UO^+.

252 In the case of Pu measurement, Pu was affected by U hydride interferences both in its elemental
253 and mono oxide forms: $^{239}Pu^{16}O$ is interfered by $^{238}U^{16}O^1H$ and ^{239}Pu is interfered by $^{238}U^1H$. The
254 influence of hydride interference is higher when the Pu content relatively to U is low. Thus, the
255 contributions of $^{238}U^{16}O^1H$ and $^{238}U^1H$ were estimated from UKMOX-100 particles containing ~1 wt%
256 of Pu. The contribution of $^{238}U^{16}O^1H$ on $^{239}Pu^{16}O$ was ~19 % and the one of $^{238}U^1H$ on ^{239}Pu was ~7 %.
257 Moreover it was previously observed that the PuO/Pu ratio was lower than the UO/U ratio[34]. Thus,
258 the contribution of $^{238}U^{16}O^1H$ is probably underestimated. In conclusion, it is recommended to measure
259 Pu in its elemental form.

260 Finally, based on the lower hydride formation rate measured for U particles, we estimated that
261 the lowest measurable Pu/U atomic ratio in MOX particles is $\sim 1.6 \times 10^{-3}$.

262

263 *3.2. Measurement of $^{240}Pu/^{239}Pu$ in pure* Pu *particles*

264 Only the major isotopic Pu ratio, $^{240}Pu/^{239}Pu$, was measured in this study. ^{241}Pu was interfered by
265 its decay product ^{241}Am and other minor Pu atomic abundances (^{242}Pu and ^{244}Pu) were too low to be
266 efficiently measured with the current analytical conditions and in the single collection mode. A possible
267 difficulty for the $^{240}Pu/^{239}Pu$ ratio measurements is associated with the ^{239}PuH contribution to the ^{240}Pu
268 signal. In the case of pure U particles, the hydride correction factor is determined by measuring the
269 ratio $N(^{239})/N(^{238}U)$ where the signal only comes from $^{238}UH^+$. For Pu particles, this methodology cannot
270 be applied because the $^{n}PuH^+$ signal cannot be distinguished from the $^{n+1}Pu^+$ signal. We assume that
271 the UH/U and PuH/Pu ratios did not significantly depend on the chemical species. This hypothesis is
272 supported by some studies in which UH/U and Pu/H ratios determined in micrometric clay spheres (~2
273 µm) containing U and Pu[42] were close.

Accordingly, we applied the UH/U ratio measured on NBS U-100 particles (made of U_3O_8) during the same analytical session to subtract the ^{239}PuH contribution to the measured ^{240}Pu/^{239}Pu atomic ratio. The accuracy of the ^{240}Pu/^{239}Pu isotopic ratio measurements with/without ^{239}PuH corrections is discussed below.

The ^{240}Pu/^{239}Pu isotopic ratio was corrected according to Equation 1:

$$\left(\frac{^{240}Pu}{^{239}Pu}\right)_{cor} = \frac{\frac{N_{240}}{N_{^{239}Pu}} - \frac{N_{^{239}Pu}\,{}^{1}H}{N_{^{239}Pu}}}{1-IMF_{amu}\times(M_{^{239}Pu}-M_{^{240}Pu})} = \frac{\frac{N_{240}}{N_{^{239}Pu}} - \frac{N_{^{238}U}\,{}^{1}H}{N_{^{238}U}}}{1-IMF_{amu}\times(M_{^{239}Pu}-M_{^{240}Pu})} \quad (1)$$

With N_{240} and N_{Pu239}: signals measured at m/z of ^{240}Pu and m/z of ^{239}Pu, respectively,

M_{Pu239} and M_{Pu240}: molar masses of ^{239}Pu and ^{240}Pu, respectively,

$\frac{N_{U238H1}}{N_{U238}}$: U hydride ratio measured on NBS U-100 particles during the same analytical session,

IMF_{amu}: Instrumental mass fractionation factor per atomic mass unit (amu) measured on NBS U-100 particles during the same analytical session.

The ^{240}Pu/^{239}Pu isotopic ratios in individual Pu particles from CMX-6 measured during three analytical sessions are presented in Fig. 2.

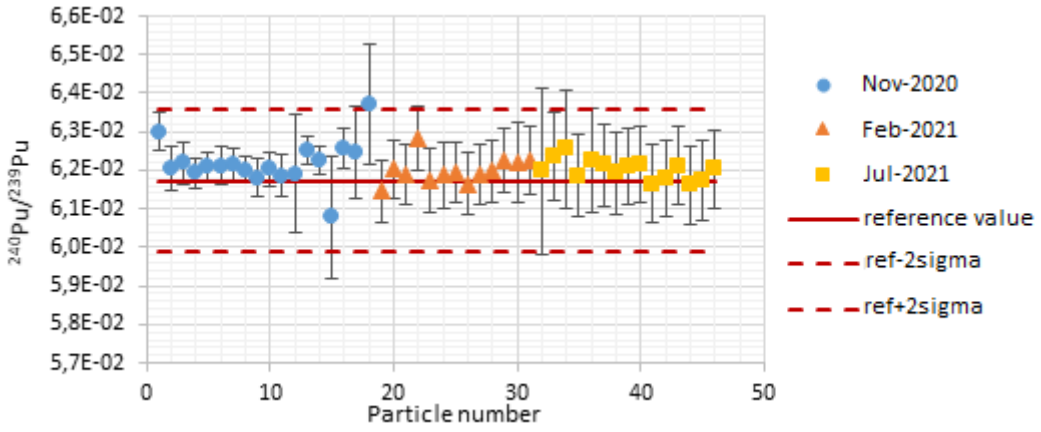

Fig. 2 ^{240}Pu/^{239}Pu isotopic ratios measured on individual CMX-6 particles in November 2020 (blue circles), in February 2021 (orange triangles) and in July 2021 (yellow squares). Expanded uncertainties

are given with a 95 % confidence level. The red line corresponds to the expected value. The red dashed lines correspond to the upper and lower uncertainties of the expected value.

For all analytical sessions, measurements were in agreement with the expected value within individual uncertainties. The average isotopic ratios for each analytical session are given in Table 3.

Table 3 Average $^{240}Pu/^{239}Pu$ atomic ratios measured on pure Pu particles from CMX-6 during three analytical sessions. Expanded uncertainties are given with a coverage factor of 2 (confidence level of 95%). Corresponding ratios without ^{239}PuH correction are also given. Values in parentheses below the atomic ratios are the relative difference with the expected ratio.

Analytical session	**November 2020**	**February 2021**	**July 2021**
$^{240}Pu/^{239}Pu$ with hydride correction	$(6.22 \pm 0.12) \times 10^{-2}$ (0.7 %)	$(6.20 \pm 0.10) \times 10^{-2}$ (0.4 %)	$(6.20 \pm 0.11) \times 10^{-2}$ (0.5 %)
$^{240}Pu/^{239}Pu$ without hydride correction	$(6.27 \pm 0.12) \times 10^{-2}$ (1.6 %)	$(6.30 \pm 0.07) \times 10^{-2}$ (2.1 %)	$(6.30 \pm 0.06) \times 10^{-2}$ (2.1 %)
Number of analysed particles	18	13	13

According to the results in Table 3, no biases was observed for the $^{240}Pu/^{239}Pu$ ratios with ^{239}PuH correction, although they are slightly above the expected ratio (relative difference of ~0.5% with respect to the expected values whereas relative expanded uncertainties are ~2%).

Assuming that the Pu hydride ratio is identical to the U hydride rate measured during the analytical sessions, the contribution of ^{239}PuH to the ^{240}Pu signal could be quantified. Depending on the session, the UH/U ratio varies between 5.5×10^{-4} and 10^{-3}. Therefore, the ^{239}PuH signal contributed to 1 to 2.4% of the signal measured at the m/z ratio of ^{240}Pu. Without hydride correction, the $^{240}Pu/^{239}Pu$ isotopic ratios presented in Table 3 is largely overestimated with respect to the expected ratio (relative differences between 1.6 % and 2.1 %).

As a conclusion, the results confirmed the relevance of the Pu hydride correction based on UH/U measurements to improve the measurement accuracy of the $^{240}Pu/^{239}Pu$ isotopic ratios.

3.3. Application to the isotopic characterisation of MOX particles

Only the $^{235}U/^{238}U$ and $^{240}Pu/^{239}Pu$ isotope ratios were measured. For the $^{240}Pu/^{239}Pu$ isotopic ratio determination, the hydride correction method described above was applied. Both ^{239}Pu and ^{240}Pu isotopes were corrected for hydride contributions (^{238}UH on ^{239}Pu and ^{239}PuH on ^{240}Pu).

For this study, particles from the two MOX samples, UKMOX-100 and UKMOX-010, were analysed. The U and Pu isotopic compositions are identical, whereas the bulk Pu/U ratios are different between the two materials (see Table 1). The $^{240}Pu/^{239}Pu$ isotopic ratio was corrected according to Equation 2:

$$\left(\frac{^{240}Pu}{^{239}Pu}\right)_{cor} = \frac{\frac{N_{240}-N_{239_{Pu}}\,{}^{1}H}{N_{239}-N_{238_U}\,{}^{1}H}}{1-IMF_{amu}\times(M_{239_{Pu}}-M_{240_{Pu}})} = \frac{\frac{N_{240}}{N_{238_U}\,{}^{1}H}-\frac{N_{238_U}\,{}^{1}H}{N_{238_U}}}{1-IMF_{amu}\times(M_{239_{Pu}}-M_{240_{Pu}})} \quad (2)$$

With $N_{240}, N_{239}\ and\ N_{U238}$: signals measured at m/z of ^{240}Pu, ^{239}Pu and ^{238}U, respectively,

$M_{Pu239}\ and\ M_{Pu240}$: molar masses of ^{239}Pu and ^{240}Pu respectively,

$\frac{N_{U238H1}}{N_{U238}}$: hydride ratio measured on NBS U-100 particles during the same analytical session,

IMF_{amu}: instrumental mass fractionation factor par amu measured on NBS U-100 particles during the same analytical session.

Two analytical sessions were performed, one for UKMOX-100 particles and one for UKMOX-010 particles. The individual $^{240}Pu/^{239}Pu$ isotopic ratios are plotted in Fig. 3, see Supplementary Information B for $^{235}U/^{238}U$ isotopic ratio results. For both analytical sessions, the results are in agreement with the expected value within individual uncertainties. The average isotopic ratios of U and Pu are given in Table 4 for each sample.

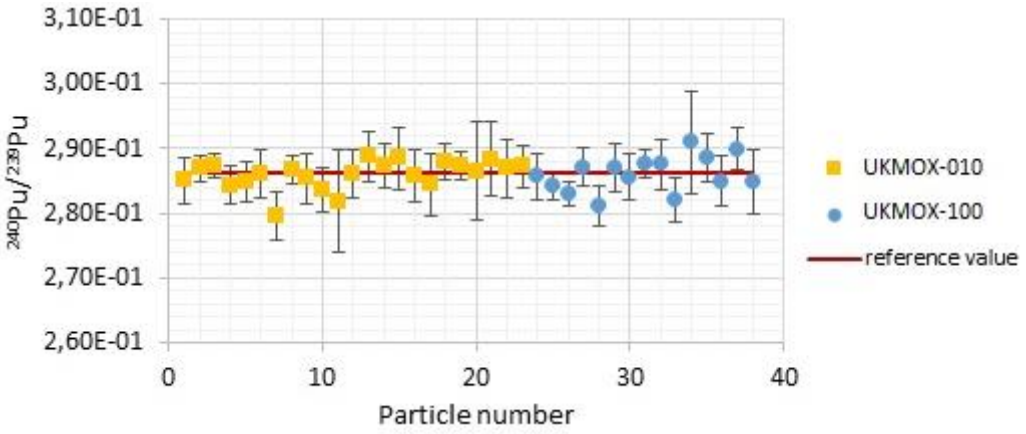

Fig. 3 $^{240}Pu/^{239}Pu$ isotopic ratios measured for individual UKMOX-010 (yellow squares) and UKMOX-100 (blue points) particles. Expanded uncertainties are given with a 95% confidence level. The red line corresponds to the reference value.

Table 4 Average $^{240}Pu/^{239}Pu$ and $^{235}U/^{238}U$ isotopic ratios measured for MOX particles. Expanded uncertainties are given with a coverage factor of 2 (confidence level of 95%). $^{240}Pu/^{239}Pu$ isotopic ratios without U and Pu hydride corrections are also given. Values in parenthesis below the atomic ratios are the relative difference with respect to the reference value.

	UKMOX-010	**UKMOX-100**
$^{240}Pu/^{239}Pu$ with U and PuH corrections	$(2.859 \pm 0.046) \times 10^{-1}$ (-0.06 %)	$(2.859 \pm 0.058) \times 10^{-1}$ (-0.03 %)
$^{240}Pu/^{239}Pu$ without UH and PuH corrections	$(2.844 \pm 0.064) \times 10^{-1}$ (-0.59 %)	$(2.749 \pm 0.12) \times 10^{-1}$ (-3.76 %)
$^{235}U/^{238}U$	$(1.590 \pm 0.031) \times 10^{-2}$ (+0.03 %)	$(1.584 \pm 0.034) \times 10^{-2}$ (-0.37 %)
Number of analysed particles	23	15

The relative expanded uncertainty is below 2 % for the two samples. Depending on the MOX sample, the contribution of the ^{238}UH to the signal at the m/z ratio of ^{239}Pu ranges from 0.9 % for UKMOX-010 to 4.2 % for UKMOX-100. This contribution is significantly higher for UKMOX-100 than for UKMOX-010 as expected because of its lower Pu content. Without ^{239}PuH correction, the $^{240}Pu/^{239}Pu$ isotopic ratio is underestimated. Although the relative difference with respect to the expected value (-

3.7 %) is slightly lower than the relative expended uncertainties (4.4 %), we conclude that a negative bias is observed for the UKMOX- 100 material when no U and Pu hydride corrections are carried out. Alsehin et al. [32] already observed such significant bias for the analysis of the same sample without hydride correction.

As a conclusion, the U and Pu hydride corrections based on U measurements improve the accuracy of $^{240}Pu/^{239}Pu$ isotopic ratios in MOX with 1 to 10 wt % of Pu.

3.4. Pu quantification in MOX particles

To quantify the Pu content in U matrix, it is necessary to determine the RSF between U and Pu. The RSF is mainly used in SIMS as a quantification factor to correlate the ionic intensity of an element to its concentration in a given matrix. This factor is calculated according to Equation 3:

$$RSF_{^{239}Pu/^{238}U} = \frac{\left(\frac{^{239}Pu}{^{238}U}\right)_{reference}}{\left(\frac{^{239}Pu}{^{238}U}\right)_{measured}} \quad (3)$$

To determine this factor, it is necessary to use a reference material with known U and Pu concentrations in a similar matrix. To the best of our knowledge, there is no available U–Pu oxide reference material certified at the particle scale. Here, we proposed a methodology to determine this factor from pure Pu particles with known purification date and isotopic ratios determined by ICP-MS measurements during the CMX-6 exercise. Equivalent methodologies for RSF determination with other isotopes, $^{239}Pu/^{235}U$ and $^{230}Th/^{234}U$, were already developed respectively for the age dating of Pu particles[45] or that of U particles[46]. The novelty of our methodology is to extrapolate a RSF measured for the ratio $^{235}U/^{239}Pu$ to the RSF used for correcting $^{239}Pu/^{238}U$ ratio. As the decay products ("daughter nuclides") of some Pu isotopes are U isotopes (^{239}Pu and ^{240}Pu decay into ^{235}U and ^{236}U, respectively), we can calculate the theoretical $^{235}U/^{239}Pu$ and $^{236}U/^{240}Pu$ atomic ratios by reversing Bateman's equation. The use of two different radio-chronometers allows verifying the absence of bias. However, this method is only valid when the Pu was perfectly purified. Otherwise, the determination of the isotopic ratio is biased by the presence of residual U. Here, we assume that (1) the number of atoms of the "daughter nuclides" (U

isotopes) after purification is zero, and that (2) the numbers of atoms of the "father" radionuclides, here Pu isotopes, did not significantly change during the elapsed time between the purification and the analysis, given the long half-lives of ^{239}Pu and ^{240}Pu. Previous measurements performed in our laboratory by means of a multiple-collector ICP-MS confirmed these hypotheses and demonstrated that the calculated model age based on ^{236}U/^{240}Pu was in agreement with the purification date. ^{235}U, ^{236}U, ^{239}Pu and ^{240}Pu signals were measured in CMX-6 particles during three analytical sessions in order to calculate RSF between Pu and U thanks to the ratios ^{240}Pu/^{236}U and ^{239}Pu/^{235}U according to Equation 3.

The final $RSF_{239Pu/238U}$ used to calculate the ^{239}Pu/^{238}U ratio for the determination of the Pu content in U was calculated according to Equation 4:

$$RSF_{^{239}Pu/^{238}U} = \frac{1}{1-IMF_{amu}\times(M_{^{238}U}-M_{^{235}U})} \times \frac{1}{RSF_{^{235}U/^{239}Pu}} \quad (4)$$

Where M_{238U} and M_{235} are the molar masses of ^{238}U and ^{235}U, respectively.

A similar equation was used for calculating $RSF_{236U/240Pu}$. The $RSF_{239Pu/238U}$ values calculated for all analytical sessions are plotted in Fig. 4. The measurements are clearly reproducible. It may also be noted that values calculated with the two U-Pu radio-chronometers are in perfect agreement. The RSF values measured in the present study are also in agreement with the those reported in the literature: (1) in U-Pu oxide particles (0.41) [29], and (2) in U-Pu-bearing clay microspheres (0.34) [42].

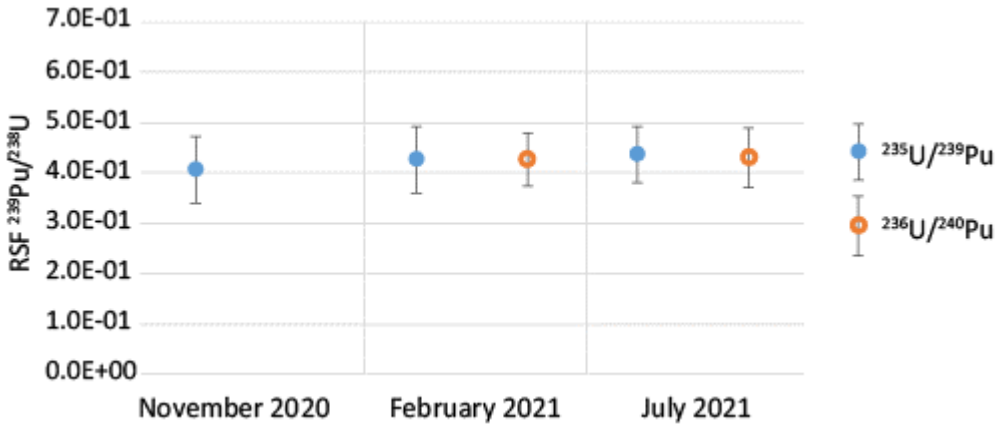

Fig. 4 Average RSF $^{239}Pu/^{238}U$ measured with the $^{235}U/^{239}Pu$ (blue point) and with the $^{236}U/^{240}Pu$ (yellow circles) radio-chronometers. Expanded uncertainties are given with a 95 % confidence level. $^{236}U/^{240}Pu$ isotopic ratio was not measured during the November 2020 analytical session.

The $RSF_{239Pu/238U}$ was then applied to MOX particles to quantify their Pu content according to Equation 5:

$$\left(\frac{^{239}Pu}{^{238}U}\right)_{corrected} = \left(\frac{^{239}Pu}{^{238}U}\right)_{measured} \times RSF_{^{239}Pu/^{238}U} \quad (5)$$

$^{239}Pu/^{238}U$ ratios measured for individual UKMOX-100 and UKMOX-010 particles are plotted in Fig. 5.

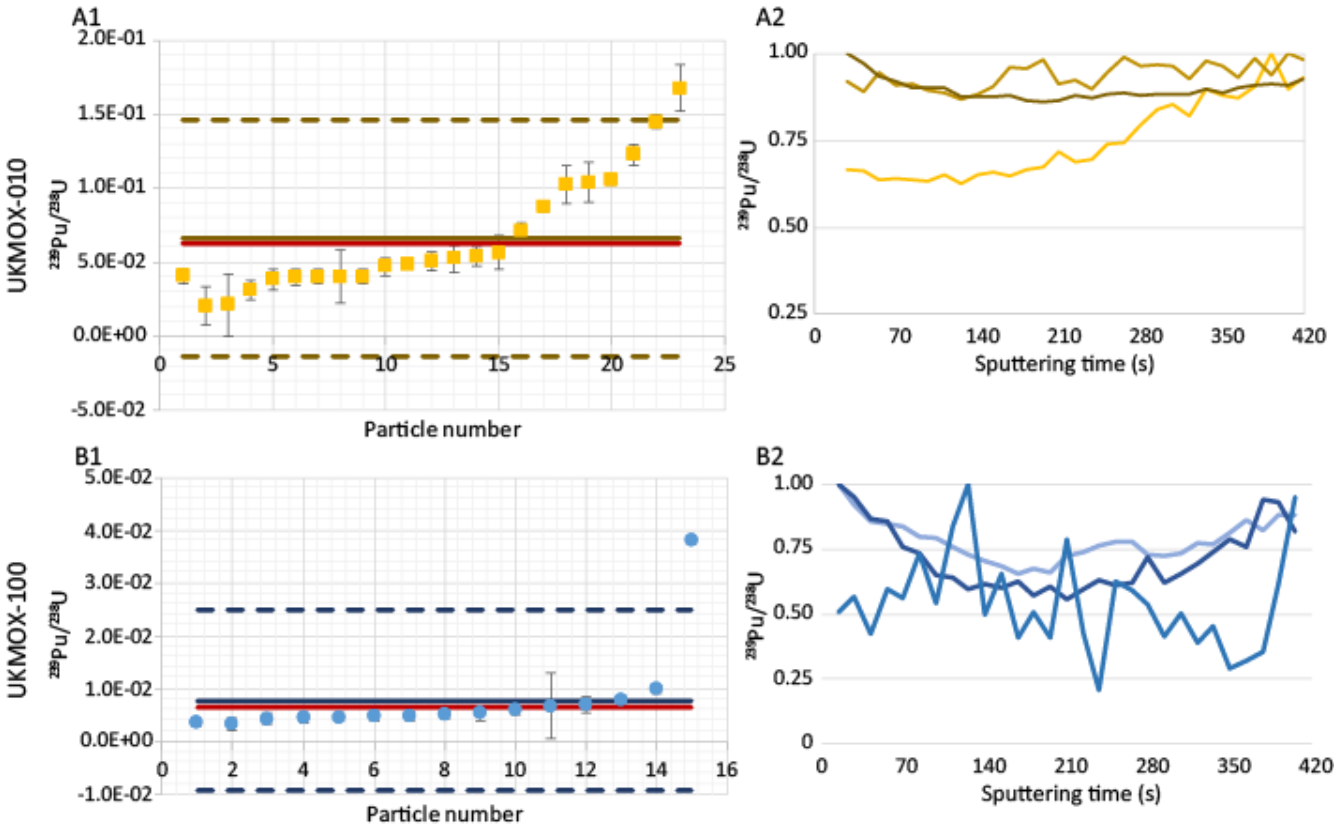

Fig. 5 $^{239}Pu/^{238}U$ isotopic ratios measured in individual particles from (A1) UKMOX-010 sample (yellow squares), and (B1) UKMOX-100 sample (blue points) (Presented in increasing ratio). Individual expanded uncertainties are given with a 95% confidence level. The red line corresponds to the reference value. The yellow and blue lines correspond to the averages of the measured ratios for both samples. The coloured dashed lines correspond to the expanded uncertainties on the average ratio.

$^{239}Pu/^{238}U$ isotopic ratios (normalized to the highest ratio) are plotted against the sputtering time for three UKMOX-010 particles (A2), and for three UKMOX-100 particles (B2).

The results presented in Fig. 5 A1 and B1 show that the average $^{239}Pu/^{238}U$ ratios normalized to the highest ratio are in agreement with the expected values within uncertainties for both MOX samples. A deviation of the $^{239}Pu/^{238}U$ ratios is observed, it linked to the heterogeneity of the Pu content in the U matrix, because the MOX forms a solid solution defined by a macroscopic homogeneity and a heterogeneity on the atomic scale. These results validate the RSF value measured in pure Pu particle. However individual $^{239}Pu/^{238}U$ ratios exhibit large variations between particles by a factor of 8 and 10 for UKMOX-010 and UKMOX-100 samples, respectively. Therefore, we observe that the U and Pu proportions in these two materials are heterogeneous at the particle scale. Moreover, $^{239}Pu/^{238}U$ ratios measured against sputtering time for three individual particles from each MOX sample showed large variations up to a factor 2 (Fig. 5A2 and 5B2). Such heterogeneities of the distributions of Pu content between and within particles were also observed by Aleshin et al in UKMOX-010 particles.

4. Conclusion

In this study, we demonstrate that it is preferable to measure U and Pu in their elemental form for MOX particle characterisation by SIMS. Indeed, mono-oxide ions are more abundant although they are also more sensitive to the isobaric interferences than elemental ions. We also developed and validated a U and Pu hydride correction (^{238}UH for ^{239}Pu and ^{239}PuH for ^{240}Pu) for the measurement of the $^{240}Pu/^{239}Pu$ atomic ratios based on the UH/U ratios measured in particles from the NBS U-100 CRM. This method was then successfully applied to MOX particles. Analyses of MOX particles showed that (1) the isotopic ratios $^{235}U/^{238}U$ and $^{240}Pu/^{239}Pu$ were in agreement with the expected values, and that (2) the hydride correction is robust for a Pu content comprised between 1 and 10 wt% in U. Lastly, we also developed and validated in this study a method for the Pu quantification in U through the use of

the RSF calculated with pure Pu particles of known purification date. These analyses demonstrated the heterogeneity of the Pu content between particles and within particles from UKMOX-010 and UKMOX-100. The method described in the current research opens the way to the isotopic characterisation of environmental particles containing U, Pu or both elements, resulting from major nuclear power plant accidents (CNPP, FDNPP, etc.), weapon accidents (Thule, Palomares, etc.), atmospheric nuclear weapon tests, potential releases from nuclear facilities, etc. Before applying this methodology to these samples, further studies are required to evaluate the impact of other potential isobaric interferences on U and Pu that can be induced by other elements coming from the particle itself or from neighboring environmental particles (e.g. mineral particles). Actually, some isobaric interferences on U isotopic measurements are well known [14] .The impact of such interferences could also be reduced by using a LG-SIMS, which enables to work with a higher mass resolution [14]. Such instrument is also equipped with a multi-collection detector arrangement that enables to collect up to five isotopes simultaneously, thereby reducing the isotopic ratio uncertainties [15]. Such device could be used to measure simultaneously the $^{235}U/^{238}U$ and $^{239}Pu/^{240}Pu$ ratios.

Acknowledgements

Aurélie Diacre received a PhD fellowship from CEA (Commissariat à l'Energie Atomique et aux Energies Alternatives, France). The authors are also grateful to M. Aleshin, T. Tanpraphan, G. Stadelman, U. Repinc, L. Sangely, and A. Bosko (IAEA, Office of Safeguards Analytical Services) for providing the MOX samples.

Author contributions

Diacre Aurélie: Writing – original draft, Investigation, Data curation. **Fauré Anne-Laure:** Writing - Review – Supervision, Data curation. **Cornaton Manon:** Supervision, Data curation. **Pointurier Fabien:** Writing - Review – Supervision. **Evrard Olivier**: Writing - Review – Supervision.

References

[1] J.A. Kelley, D.A. Jaffe, A. Baklanov, A. Mahura, Heavy metals on the Kola Peninsula: aerosol size distribution, Science of The Total Environment. 160–161 (1995) 135–138. https://doi.org/10.1016/0048-9697(95)04351-Z.

[2] B. Chen, A.F. Stein, P.G. Maldonado, A.M. Sanchez de la Campa, Y. Gonzalez-Castanedo, N. Castell, J.D. de la Rosa, Size distribution and concentrations of heavy metals in atmospheric aerosols originating from industrial emissions as predicted by the HYSPLIT model, Atmospheric Environment. 71 (2013) 234–244. https://doi.org/10.1016/j.atmosenv.2013.02.013.

[3] E. Kuhn, D. Fischer, M. Ryjinski, Environmental Samplig for IAEA Safeguards: A five year review, Vienne, 2001.

[4] A.J. Pidduck, M.R. Houlton, G.M. Williams, D.L. Donohue, Micro-analytical characterization of Uranium particles in support of environmental sampling for safeguards, (2006).

[5] D.L. Donohue, Strengthening IAEA safeguards through environmental sampling and analysis, Journal of Alloys and Compounds. 271–273 (1998) 11–18. https://doi.org/10.1016/S0925-8388(98)00015-2.

[6] F. Esaka, M. Magara, C.G. Lee, S. Sakurai, S. Usuda, N. Shinohara, Comparison of ICP-MS and SIMS techniques for determining uranium isotope ratios in individual particles, Talanta. 78 (2009) 290–294. https://doi.org/10.1016/j.talanta.2008.11.011.

[7] S. Baude, M.C. Lanière, O. Marie, Micrometrie particle's isotopics: An ultra-sensitive tool to detect nuclear plant discharge in the environment, in: 2002. IAEA-SM-367-10105.

[8] C.G. Lee, K. Iguchi, J. Inagawa, D. Suzuki, F. Esaka, M. Magara, S. Sakurai, K. Watanabe, S. Usuda, Development in fission track-thermal ionization mass spectrometry for particle analysis of safeguards environmental samples, J Radioanal Nucl Chem. 272 (2007) 299–302. https://doi.org/10.1007/s10967-007-0519-0.

[9] V. Stebelkov, I. Elantyev, M. Hedberg, M. Wallenius, A.-L. Fauré, Determination of isotopic composition of uranium in the CMX-4 samples by SIMS, J Radioanal Nucl Chem. 315 (2018) 417–423. https://doi.org/10.1007/s10967-017-5664-5.

[10] A.-L. Fauré, C. Rodriguez, O. Marie, J. Aupiais, F. Pointurier, Detection of traces of fluorine in micrometer sized uranium bearing particles using SIMS, J. Anal. At. Spectrom. 29 (2013) 145–151. https://doi.org/10.1039/C3JA50245G.

[11] P.M.L. Hedberg, P. Peres, J.B. Cliff, F. Rabemananjara, S. Littmann, H. Thiele, C. Vincent, N. Albert, Improved particle location and isotopic screening measurements of sub-micron sized particles by Secondary Ion Mass Spectrometry, J. Anal. At. Spectrom. 26 (2011) 406–413. https://doi.org/10.1039/C0JA00181C.

[12] P. Peres, P.M.L. Hedberg, S. Walton, N. Montgomery, J.B. Cliff, F. Rabemananjara, M. Schuhmacher, Nuclear safeguards applications using LG-SIMS with automated screening capabilities: Nuclear safeguards applications using LG-SIMS, Surf. Interface Anal. 45 (2013) 561–565. https://doi.org/10.1002/sia.5015.

[13] P.M.L. Hedberg, P. Peres, F. Fernandes, N. Albert, C. Vincent, Latest improvements in isotopic uranium particle analysis by large geometry–secondary ion mass spectrometry for nuclear safeguards purposes, Journal of Vacuum Science & Technology B. 36 (2018) 03F108. https://doi.org/10.1116/1.5016943.

[14] Y. Ranebo, P.M.L. Hedberg, M.J. Whitehouse, K. Ingeneri, S. Littmann, Improved isotopic SIMS measurements of uranium particles for nuclear safeguard purposes, J. Anal. At. Spectrom. 24 (2009) 277. https://doi.org/10.1039/b810474c.

[15] P.M.L. Hedberg, P. Peres, F. Fernandes, L. Renaud, Multiple ion counting measurement strategies by SIMS – a case study from nuclear safeguards and forensics, Journal of

505 Analytical Atomic Spectrometry. 30 (2015) 2516–2524.
506 https://doi.org/10.1039/C5JA00382B.
507 [16] A.-L. Fauré, T. Dalger, Age Dating of Individual Micrometer-Sized Uranium Particles by
508 Secondary Ion Mass Spectrometry: An Additional Fingerprint for Nuclear Safeguards
509 Purposes, Anal. Chem. 89 (2017) 6663–6669.
510 https://doi.org/10.1021/acs.analchem.7b00887.
511 [17] F. Pointurier, O. Marie, Identification of the chemical forms of uranium compounds in
512 micrometer-size particles by means of micro-Raman spectrometry and scanning electron
513 microscope, Spectrochimica Acta Part B: Atomic Spectroscopy. 65 (2010) 797–804.
514 https://doi.org/10.1016/j.sab.2010.06.008.
515 [18] M.C. Jiménez-Ramos, R. García-Tenorio, I. Vioque, G. Manjón, M. García-León,
516 Presence of plutonium contamination in soils from Palomares (Spain), Environmental
517 Pollution. 142 (2006) 487–492. https://doi.org/10.1016/j.envpol.2005.10.030.
518 [19] O.C. Lind, B. Salbu, K. Janssens, K. Proost, H. Dahlgaard, Characterization of uranium
519 and plutonium containing particles originating from the nuclear weapons accident in
520 Thule, Greenland, 1968, Journal of Environmental Radioactivity. 81 (2005) 21–32.
521 https://doi.org/10.1016/j.jenvrad.2004.10.013.
522 [20] B. Salbu, V. Kashparov, O.C. Lind, R. Garcia-Tenorio, M.P. Johansen, D.P. Child, P.
523 Roos, C. Sancho, Challenges associated with the behaviour of radioactive particles in the
524 environment, Journal of Environmental Radioactivity. 186 (2018) 101–115.
525 https://doi.org/10.1016/j.jenvrad.2017.09.001.
526 [21] P.R. Danesi, J. Moreno, M. Makarewicz, Z. Radecki, Residual radioactivity in the
527 terrestrial environment of the Mururoa and Fangataufa Atolls nuclear weapon test sites,
528 Journal of Radioanalytical and Nuclear Chemistry. 253 (2002) 13. https://doi.org/0236–
529 5731/2002/USD 17.00.
530 [22] F.J. Sandalls, M.G. Segal, N. Victorova, Hot particles from Chernobyl: A review, Journal
531 of Environmental Radioactivity. 18 (1993) 5–22. https://doi.org/10.1016/0265-
532 931X(93)90063-D.
533 [23] E. Kurihara, M. Takehara, M. Suetake, R. Ikehara, T. Komiya, K. Morooka, R. Takami,
534 S. Yamasaki, T. Ohnuki, K. Horie, M. Takehara, G.T.W. Law, W. Bower, J.F. W.
535 Mosselmans, P. Warnicke, B. Grambow, R.C. Ewing, S. Utsunomiya, Particulate
536 plutonium released from the Fukushima Daiichi meltdowns, Science of The Total
537 Environment. 743 (2020) 140539. https://doi.org/10.1016/j.scitotenv.2020.140539.
538 [24] M. Eriksson, K. Ljunggren, C. Hindorf, Plutonium hot particle separation techniques using
539 real-time digital image systems, Nuclear Instruments and Methods in Physics Research
540 Section A: Accelerators, Spectrometers, Detectors and Associated Equipment. 488 (2002)
541 375–380. https://doi.org/10.1016/S0168-9002(02)00438-2.
542 [25] S.V. Shevchenko, On the uncertainty in activity measurements for samples containing
543 “hot particles,” Applied Radiation and Isotopes. 61 (2004) 1303–1306.
544 https://doi.org/10.1016/j.apradiso.2004.02.022.
545 [26] M.C. Jiménez-Ramos, J. García-López, R. García-Tenorio, M. García-León,
546 Characterization of terrestrial hot particles from the Palomares accident using destructive
547 and non-destructive analytical techniques, Radioprotection. 44 (2009) 345–350.
548 https://doi.org/10.1051/radiopro/20095067.
549 [27] V. Tcherkezian(Cherkezyan), V. Shkinev, L. Khitrov, G. Kolesov, Experimental approach
550 to chernobyl hot particles, Journal of Environmental Radioactivity. 22 (1994) 127–139.
551 https://doi.org/10.1016/0265-931X(94)90018-3.
552 [28] J.A. Entwistle, A.G. Flowers, G. Nageldinger, J.C. Greenwood, Identification and
553 characterization of radioactive ‘hot’ particles in Chernobyl fallout-contaminated soils: the

554 application of two novel approaches, Mineral. Mag. 67 (2003) 183–204.
555 https://doi.org/10.1180/0026461036720094.
556 [29] M. Wallenius, K. Lützenkirchen, K. Mayer, I. Ray, L.A. de las Heras, M. Betti, O.
557 Cromboom, M. Hild, B. Lynch, A. Nicholl, H. Ottmar, G. Rasmussen, A. Schubert, G.
558 Tamborini, H. Thiele, W. Wagner, C. Walker, E. Zuleger, Nuclear forensic investigations
559 with a focus on plutonium, Journal of Alloys and Compounds. 444–445 (2007) 57–62.
560 https://doi.org/10.1016/j.jallcom.2006.10.161.
561 [30] M. Betti, G. Tamborini, L. Koch, Use of Secondary Ion Mass Spectrometry in Nuclear
562 Forensic Analysis for the Characterization of Plutonium and Highly Enriched Uranium
563 Particles, Anal. Chem. 71 (1999) 2616–2622. https://doi.org/10.1021/ac981184r.
564 [31] Y. Ranebo, N. Niagolova, N. Erdmann, M. Eriksson, G. Tamborini, M. Betti, Production
565 and Characterization of Monodisperse Plutonium, Uranium, and Mixed
566 Uranium−Plutonium Particles for Nuclear Safeguard Applications, Anal. Chem. (2010).
567 https://doi.org/10.1021/ac9029295.
568 [32] M. Aleshin, T. Tanpraphan, O. Bildstein, L. Sangely, U. Repinc, A. Bosko, J. Poths, S.
569 Vogt, Y. Kuno, Isotopic analysis of U-PU mixed particles using Large-Geometry
570 Secondary Ion Masse Spectrometer (LG-SIMS), (2019).
571 https://www.iaea.org/sites/default/files/19/07/cn-267-book-of-abstracts.pdf.
572 [33] J.J. Bellucci, M.J. Whitehouse, M. Aleshin, M. Eriksson, Simultaneous Pu and U Isotope
573 Nuclear Forensics on an Environmentally Recovered Hot Particle, Anal. Chem. 91 (2019)
574 5599–5604. https://doi.org/10.1021/acs.analchem.8b04809.
575 [34] Y. Ranebo, M. Eriksson, G. Tamborini, N. Niagolova, O. Bildstein, M. Betti, The Use of
576 SIMS and SEM for the Characterization of Individual Particles with a Matrix Originating
577 from a Nuclear Weapon, Microscopy and Microanalysis. 13 (2007) 179–190.
578 https://doi.org/10.1017/S1431927607070353.
579 [35] G. Tamborini, M. Wallenius, O. Bildstein, L. Pajo, M. Betti, Development of a SIMS
580 Method for Isotopic Measurements in Nuclear Forensic Applications, Microchimica Acta.
581 139 (2002) 185–188. https://doi.org/10.1007/s006040200059.
582 [36] P. Morrall, D.W. Price, A.J. Nelson, W.J. Siekhaus, E. Nelson, K.J. Wu, M. Stratman, W.
583 McLean, ToF-SIMS characterization of uranium hydride, Philosophical Magazine Letters.
584 87 (2007) 541–547. https://doi.org/10.1080/09500830701286227.
585 [37] F. Esaka, K. Watanabe, T. Onodera, C.-G. Lee, M. Magara, S. Sakurai, S. Usuda,
586 Dependence of the precision of uranium isotope ratio on particle diameter in individual
587 particle analysis with SIMS, Applied Surface Science. 255 (2008) 1512–1515.
588 https://doi.org/10.1016/j.apsusc.2008.05.110.
589 [38] V. Radulović, A. Kolšek, A.-L. Fauré, A.-C. Pottin, F. Pointurier, L. Snoj, Qualification
590 of heavy water based irradiation device in the JSI TRIGA reactor for irradiations of FT-
591 TIMS samples for nuclear safeguards, Nuclear Instruments and Methods in Physics
592 Research Section A: Accelerators, Spectrometers, Detectors and Associated Equipment.
593 885 (2018) 139–144. https://doi.org/10.1016/j.nima.2017.12.046.
594 [39] K.T. Esaka, F. Esaka, J. Inagawa, K. Iguchi, C.-G. Lee, S. Sakurai, K. Watanabe, S. Usuda,
595 Application of Fission Track Technique for the Analysis of Individual Particles
596 Containing Uranium in Safeguard Swipe Samples, Jpn. J. Appl. Phys. 43 (2004) L915.
597 https://doi.org/10.1143/JJAP.43.L915.
598 [40] A. Diacre, P. Fichet, P. Sardini, J. Donnard, A.-L. Fauré, O. Marie, K. Shozugawa, M.
599 Susset, M. Hori, T. Tsutomu, F. Pointurier, O. Evrard, Comparison of techniques to
600 localise U-bearing particles in environmental samples, Journal of Radioanalytical and
601 Nuclear Chemistry. (2022). https://doi.org/10.1007/s10967-022-08229-w.
602 [41] D.L. Donohue, Environmental analysis, advances and future trends, (n.d.).
603 https://doi.org/IAEA-CN-184/1559.

[42] J.J. Stoffel(s), J.K. Briant, D.S. Simons, A particulate isotopic standard of uranium and plutonium in an aluminosilicate matrix, J. Am. Soc. Mass Spectrom. 5 (1994) 852–858. https://doi.org/10.1016/1044-0305(94)87008-X.
[43] Y. Ranebo, N. Niagolova, N. Erdmann, M. Eriksson, G. Tamborini, M. Betti, Production and Characterization of Monodisperse Plutonium, Uranium, and Mixed Uranium−Plutonium Particles for Nuclear Safeguard Applications, (2010). https://doi.org/10.1021/ac9029295.
[44] D.S. Simons, J.D. Fassett, Measurement of uranium-236 in particles by secondary ion mass spectrometry, J Anal At Spectrom. 32 (2017) 393–401. https://doi.org/10.1039/C6JA00402D.
[45] M. Wallenius, G. Tamborini, L. Koch, The “age” of plutonium particles, Radiochimica Acta. 89 (2001) 55–58. https://doi.org/10.1524/ract.2001.89.1.055.
[46] C. Szakal, D.S. Simons, J.D. Fassett, A.J. Fahey, Advances in age-dating of individual uranium particles by large geometry secondary ion mass spectrometry, Analyst. 144 (2019) 4219–4232. https://doi.org/10.1039/C9AN00774A.